Available online at www.sciencedirect.com

jmr&t Journal of Materials Research and Technology

https://www.journals.elsevier.com/journal-of-materials-research-and-technology

Original Article

Lightweight 3D printed Ti6Al4V-AlSi10Mg hybrid composite for impact resistance and armor piercing shielding

Ramin Rahmani[a,b,*], *Maksim Antonov*[a], *Miha Brojan*[b]

[a] *Department of Mechanical and Industrial Engineering, Tallinn University of Technology, Ehitajate tee 5, 19086 Tallinn, Estonia*

[b] *Laboratory for Nonlinear Mechanics, Faculty of Mechanical Engineering, University of Ljubljana, Askerceva 6, SI-1000 Ljubljana, Slovenia*

ARTICLE INFO

Article history:
Received 16 August 2020
Accepted 24 September 2020
Available online 7 October 2020

Keywords:
Selective laser melting
Spark plasma sintering
Armor piercing shielding
Finite element analysis

ABSTRACT

In this research, metallic lightweight ductile composites made from Ti and Al alloys are tested against dynamic impact. 3D printed Ti6Al4V cellular lattice structures with different strut diameters and cell sizes were sintered inside an AlSi10Mg powder during the low-pressure low-temperature process and investigated experimentally and analytically. Four novelties of the present study are: (1) Ti6Al4V-AlSi10Mg composite with local or overall impact reinforcement, (2) combination of selective laser melting (SLM) and spark plasma sintering (SPS) techniques to produce hybrid composites, (3) multiple impact test method with *in-situ* monitoring of sample acceleration, (4) coupling of *SolidWorks* and *ANSYS* finite element software to model and simulate penetration depth, stress distribution, deformation of uniform and gradient architecture lattices due to projectile impact. The volume fraction of the Ti6Al4V lattice (influenced by cell size and strut diameter) has a pivotal role in impact resistance. The results show that composites with smaller cell size with thinner strut diameter has similar performance to those with larger cell size with thicker struts, due to equal volume fraction. The good performance of the thickest strut possible per unit cell demonstrates the pivotal role and direct relationship of the volume fraction of the Ti6Al4V lattice for the impact resistance. In addition, the simulation results show that a *uniform* lattice structure with a higher volume fraction leads to a shallow penetration, while a *gradient* lattice hinders shape distortion.

1. Introduction

In recent years, the development of impact resistant (IR) and armor piercing (AP) shielding composites, which protect against heavier impacts and penetrating objects, has focused on lighter structures made of metals, metal-metal hybrids, ceramics, ceramic-metal (cermet), and fiber composites. Helmets, body armors, and ballistic vests are usually made of synthetic fibers such as Kevlar and metals, such as steel and titanium. The key role of these materials is to distribute and absorb the kinetic energy of the penetrating object on impact.

* *Corresponding author.*
E-mails: ramin.rahmaniahranjani@taltech.ee, ramin.rahmaniahranjani@gmail.com (R. Rahmani).

https://doi.org/10.1016/j.jmrt.2020.09.108

The ceramic and non-metallic composites or hybrids containing different materials, such as ceramic tiles can be integrated into the shield relatively easily. In such a structure, ceramics contribute to efficiency through their high hardness, compressive strength, and low density. The most widely used ceramics are Alumina (Al_2O_3), Boron Carbide (B_4C), Silicon Carbide (SiC), and Boron-Silicon Carbide. On the other hand, they have several disadvantageous properties, such as low tensile strength (low bending strength) and high melting point (high-temperature sintering equipment is required). They also have lower ductility compared to Ti and Al metals (for example), but this can be improved by advantageous properties when combined in a composite structure. As the state of the art of AP shielding, the functionality of metal-ceramic plates in ballistic armors is to safeguard against the penetration of projectiles by breaking their tips, damping the impact energy, and disrupting the propagation of penetrating fragments. In [1] Ti6Al4V titanium alloy plates, rolled and annealed by different heat treatments are subjected to ballistic impact (12.70 mm AP bullet). A microscale failure mechanism analysis was performed, and the results showed varied brittle fragmentation to ductile hole formation depending on the heat treatment parameters. In another study [2], AA6070 aluminum alloy, heat treated in different tempers suggest that aluminum alloys have a comparable perforation resistance (7.62 mm AP bullet) and strength to that of steels when region mass is considered. The current research borrows this idea and simultaneously applies Ti and Al alloys to induce lightness and strength of metal-based structures, on the condition that the metals consolidate, embed each other and assemble in a layer-by-layer mode.

With the advancement of additive powder-based technology more complex and sophisticated mixed-material composites can be fabricated. A wealth of literature is already available on this subject, covering the typical design of cellular structures (strut diameter and pore size, cell architecture, topology optimization), mechanical properties (orientation/location dependence, microstructure/phase investigation, fracture toughness, tensile strength, fatigue, etc.), metal powders or alloys (thermal deformation, solidification, etc.), printing parameters and industrial applications, see e.g. [3–8], but the literature on the response of these materials under static or dynamic impact conditions is still very scarce. In [9], for example, additively manufactured and heat-treated AlSi10Mg in a horizontal and vertical orientation and transtrack and inter-layer fracture is investigated when subjected to impact. The porosity and mechanical properties of large-scale components for aerospace applications are also investigated under impact [10]. The microanalysis of the morphology and composition of Ti6Al4V was investigated by ultrasonic impact treatment in the air with a duration of 30–150 s and leads to the formation of an amorphous layer of oxidation mixed with a separation of Fe, Al, and V [11]. Multiple sliding impacts of Ti6Al4V by ultrasonic impact treatment are induced to increase fatigue strength and prolonged lifetime [12].

Nowadays, additive manufacturing includes the term *3D printing*, which is attracting a lot of attention and opening possibilities to a wide range of novel applications, e.g. hard materials [13], tissue engineering [14], antibacterial [15], biomaterial [16], devices for in-vivo or in-vitro medical applications [17], etc. The selective laser melting (SLM) process enables manufacturing of lightweight, gradient, porous and complex geometries, of metal, ceramic and composite structures and prototyping. During the SLM process, a thin spread of powder (spherical particles) is selectively melted by a focused laser or beam additively, layer-by-layer (usually between 25 μm and 100 μm, depending on the particle size) to obtain a near-net-shape product. The melted areas of the two adjacent layers are joined together after a high cooling rate (approximately 10^5 K/s) [18,19]. Spark plasma sintering (SPS) is a comparatively new process in powder metallurgy, which allows the fabrication of bulk materials from powders, using a fast heating rate (up to 1000 °C/min) and various holding times (depending on the material phases) at high sintering temperatures (up to 2000 °C) at relatively low pressure (up to 100 MPa) and is widely applicable, ranging from metals and ceramics to cermets. During the SPS process, a high pulsed electric current is applied to the electrodes and discharges in the gaps between the powder particles to generate plasma which leads to sintering [20,21]. Graphite, as a very good electric conductor, can be used for cylindrical molds in different diameters (usually 10–100 mm) that can be applied for keeping powders or a mix of powders inside the structures in the SPS vacuum chamber. SPS is near the fully-densified process and depends on the powder sizes and SPS parameters (temperature, time, and pressure) during the process.

SLM and SPS processes individually have excellent properties, such as fully dense parts manufacturing; relatively new and operator/software friendly techniques, prototyping before mass production, near-net-shape finishing, and a wide range of metals and ceramics that can be used are the main advantage points of both processes. This motivated us to apply a combination of SLM-SPS techniques to IR and AP shielding applications, especially to fabricate metal hybrid composites for local reinforcement of the component (part). The combination of SLM-SPS approaches provides the desired shapes, thicknesses, and configurations of the Ti-Al alloys. A Ti6Al4V lattice embedded in an AlSi10Mg matrix or vice versa is a novel solution to achieve the strength of Ti, the ductility of Al, and the lightness of both together. Different cell sizes and strut diameters lead to the different volume fraction of Ti and Al alloys in the hybrid composition. In addition, this study proposes to continue with a Ti6Al4V printed lattice (metallic layer made by SLM), fill it by Al_2O_3 sintered (ceramic layer made by SPS), and fabricate a gradient structure design.

Since the price of experiments to test the collision, explosion, and destruction resistance of new materials is usually very high, the need for precise modeling and simulation tools is very important. Some studies have shown that simulations can be a valuable part of the development process. For example, in [22] the explicit dynamic finite element analysis (FEA) was implemented in ABAQUS to compare numerical predictions and experimental results. LS-DYNA software was used to measure the depth of penetration (DOP) and the design of thin, light, and inexpensive metal-ceramic armor in [23]. In [24] the monolithic and layered plate simulation against varying shank diameter showed an increase of the structural resistance with increasing projectile diameter. This important result showed a better resistance of monolithic systems.

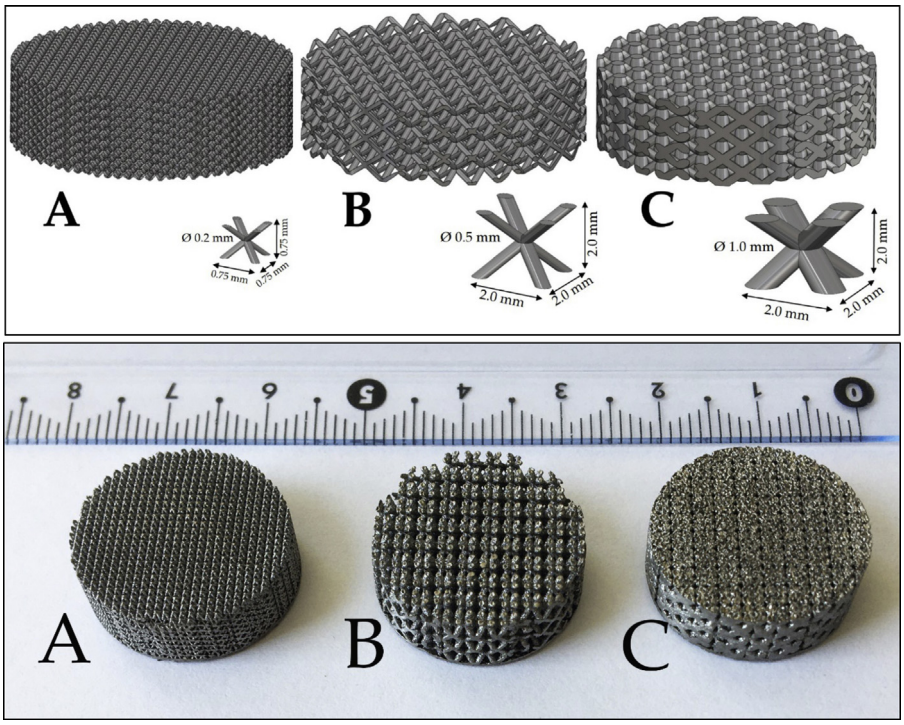

Fig. 1 – Top figure: CAD model of BCC lattice configuration and related cell size with four cross-sectional struts for A) 0.2 mm B) 0.5 mm, and C) 1.0 mm strut diameter. The diameter of each sample is 20 mm and height is 6 mm; Bottom figure: Ti6Al4V lattice structures manufactured by SLM with strut diameter, unit cell size, metal volume fraction and weight A) 0.2 mm, 0.75 mm, 37% and 3.11 g; B) 0.5 mm, 2.0 mm, 30% and 2.46 g; C) 1.0 mm, 2.0 mm, 71% and 5.91 g.

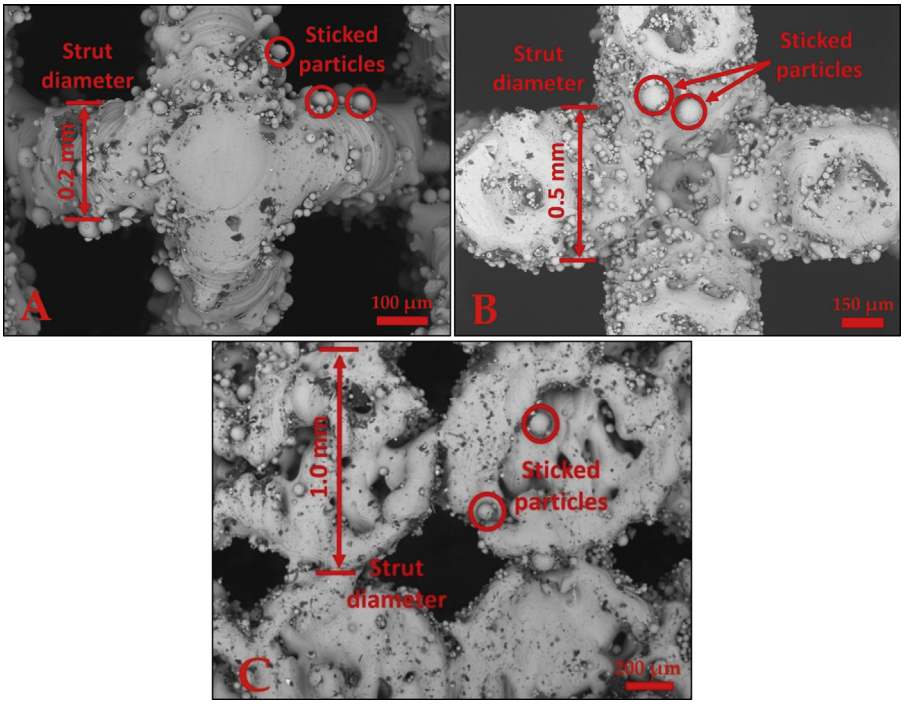

Fig. 2 – SEM micrograph of Ti6Al4V lattice with strut diameters: A) 0.2 mm, B) 0.5 mm and C) 1.0 mm.

Accordingly, an improvement of the layered shield walls from conventional layered plates to monolithic embedded layers made by a combination of layers seems necessary. It was shown in [25], that an armor system made of a single material can be resistant to the impact of small caliber projectiles, but a multi-component target comprising hard-faced ceramics, backing composites, and ductile materials can be widely used against larger caliber projectiles. The models like Johnson-

Cook and Johnson-Holmquist were used for projectile survey and materials behavior before specific software were developed. For example, the Johnson-Cook model was used for a monolithic titanium block with an impact velocity of 2000 m/s in [26].

In this article, we present a novel hybrid composite material consisting of a Ti6Al4V lattice filled with AlSi10Mg, with relatively high densification and consolidation, instead of laminated metals with adhesive layers. The use of additive manufacturing eliminates delamination and layer debonding problems, and the design of the lattice architecture contributes to higher impact absorption, which is demonstrated experimentally by capturing the zirconia ball impacts. SLM-SPS combined approaches (advanced processes of additive manufacturing and powder metallurgy) are applied to produce metal-based composites with local (desired zones) or overall (throughout the sample) reinforcement. The effect of cell and strut sizes of lattices is evaluated by a developed ball-on-plate impact test. It is shown that with the same volume fraction range, denser cell size with thinner strut diameter and courser cell size with thicker strut has almost identical depth of penetration. The experimental part of the present study is focused on impact resistance (IR) composite, however, as an application in the simulation section, armor piercing (AP) shielding is targeted. Combined *SolidWorks-ANSYS* FEA is applied to simulate the ability of gradient and uniform lattice structures against projectile impact. It is illustrated that the uniform lattice is resistant to projectile penetration/perforation, while the gradient lattice is resistant to distortion/deformation.

2. Materials and methods

An SLM50 device (from SLM solutions [27]) with laser power of 75 W, laser current of 3000 mA, exposure time 600 μs, point distance 1 μm was used to fabricate a varied unit cell size (functionally graded lattices, FGL), [28,29]. Lattices with three different strut diameters were made from Ti6Al4V material, see Fig. 1.

Strut diameter and unit cell size of the lattice are two characteristic parameters that can define/control the volume fraction of the lattice and matrix that is integrated into the free spaces between the lattice. In this study, the body-centered cubic (BCC) lattice configuration is considered for

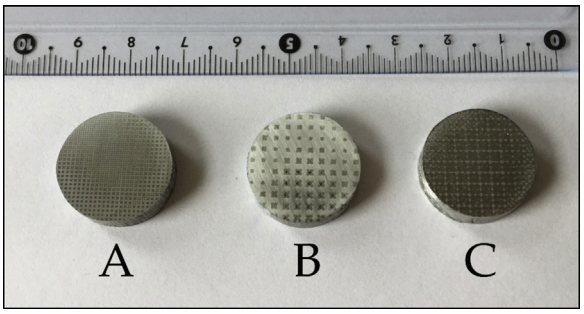

Fig. 3 – Ti6Al4V lattice filled by AlSi10Mg matrix and sintered in SPS. Lattice strut diameter and final weight of composites are: A) 0.2 mm and 4.84 g, B) 0.5 mm and 4.23 g, C) 1.0 mm and 6.40 g. The diameter of each sample is 20 mm and densification are ≈ 75-80 %.

experimental and analytical tests [30,31]. This BCC strut-based lattice is easy to define for SLM software (in case of complex structures) and flexible/deformable during the impact (in the case of high-velocity projectiles). Also, unmelted/sticked particles during the SLM process influence the weight, precision and roughness of the struts, but they can be blasted by alumina nanoparticles during post-processing. With smaller strut diameters, sticked/unmelted particles are less common; for example, 0.5 mm strut has more sticked particle than 0.2 mm strut. However, with a strut diameter of 1.0 mm or more, the structure behaves like a plain volume which unmelted particles will be covered by next layers (Fig. 2).

The spark plasma sintering (SPS, from FCT Systeme GmbH device, [32]) setup with the vacuum chamber is kept inside the nitrogen glovebox to avoid oxygen contamination during the consolidation of AlSi10Mg inside Ti6Al4V to manufacture hybrid composite [33]. The three samples are sintered at 500 °C, 5 min holding time, and 15 MPa pressure inside a 20 mm graphite mold. Experience has shown that it is preferable to hold the samples for 5 min at 300 °C and 5 MPa during the SPS process for the reduction of the oxide layer. Fig. 3 shows the result of the SPS process. Due to the low-pressure (to avoid the deformation of the lattice architecture) and the low-temperature (to avoid complete melting of the aluminum) the samples have almost the same height as modeled (as a printed Ti6Al4V lattice).

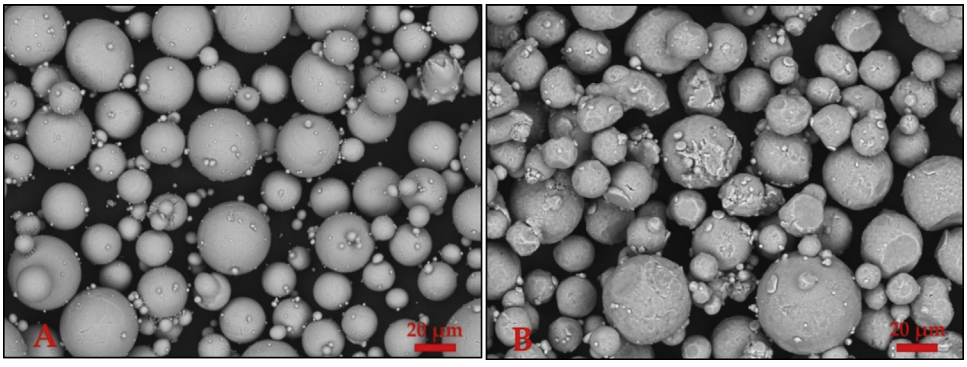

Fig. 4 – SEM micrograph of A) Ti6Al4V, B) AlSi10Mg powders.

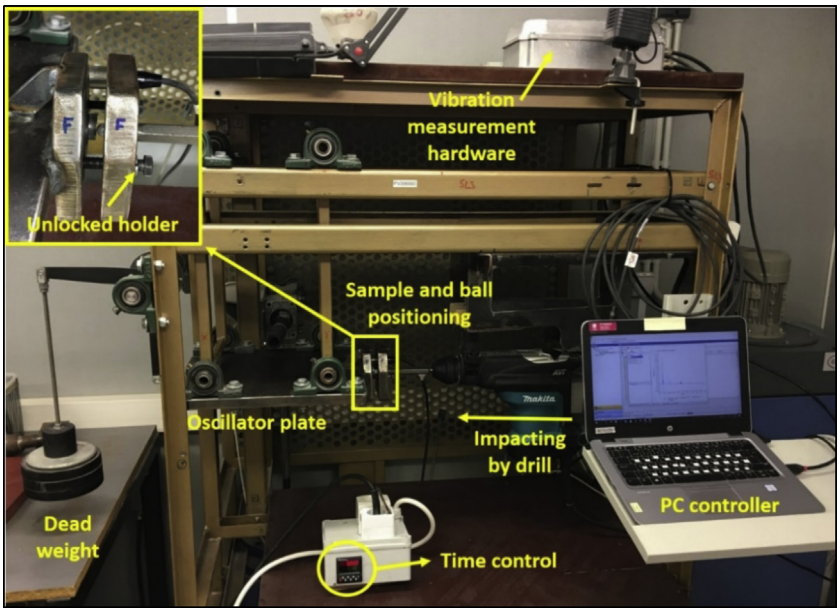

Fig. 5 – Impact test device.

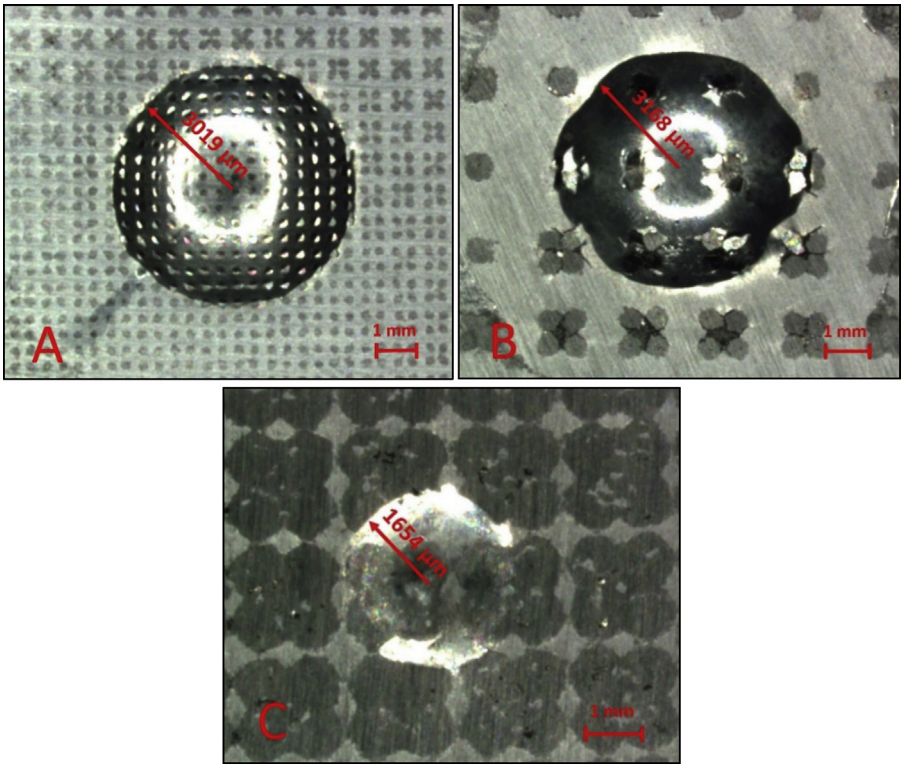

Fig. 6 – Optical images of regions formed after multiple dynamic impacts for samples with A) 0.2 mm, B) 0.5 mm, and C) 1.0 mm strut diameters.

Gas atomized Ti6Al4V Gd5 powders with the particle size $\leq$ 45 µm and a density of 4.43 g/cm^3 (supplied by TLS Technik GmbH) were used to fabricate the lattice and spherical AlSi10Mg powders with the size 20–63 µm and a density of 2.59 g/cm^3 (from the same supplier) were used for the ductile impact absorber matrix, filled by SPS into the free spaces of the lattice structure (see Fig. 4, Ti6Al4V is approximately 60 % denser than AlSi10Mg). Digital micrographs of the samples and powders were obtained using a scanning electron microscope (SEM, Zeiss EVO MA 15, Carl Zeiss AG).

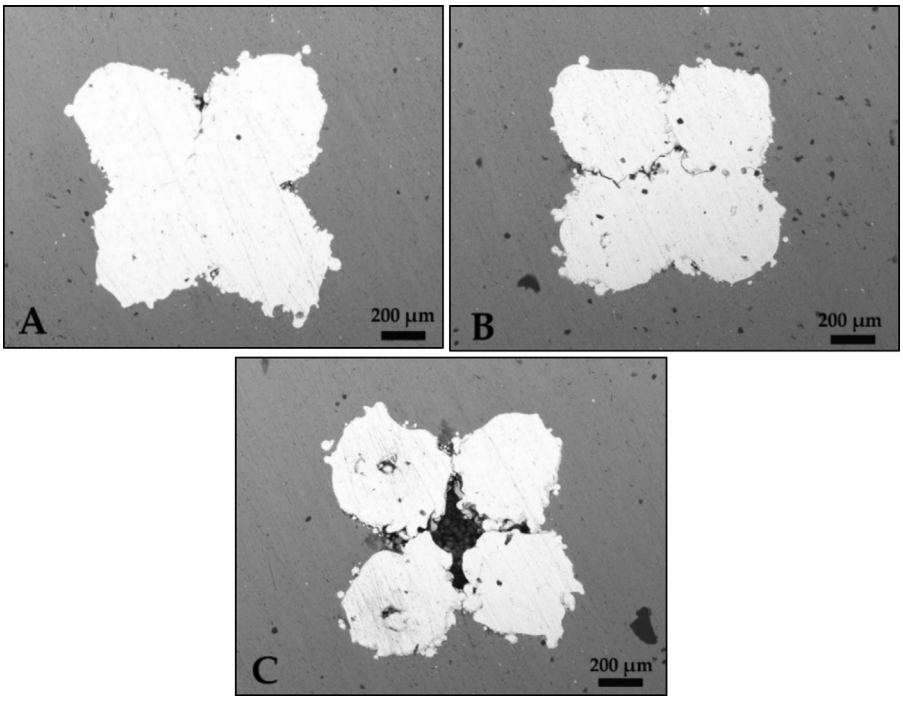

Fig. 7 – Openness of Ti6Al4V lattice located: A) far away, B) close to, C) at the edge and inside (highly affected by impact) impact region. Strut diameter is 0.5 mm (See Fig. 6B) and black region from top view is unmelted particles covering strut surface (See Fig. 2B).

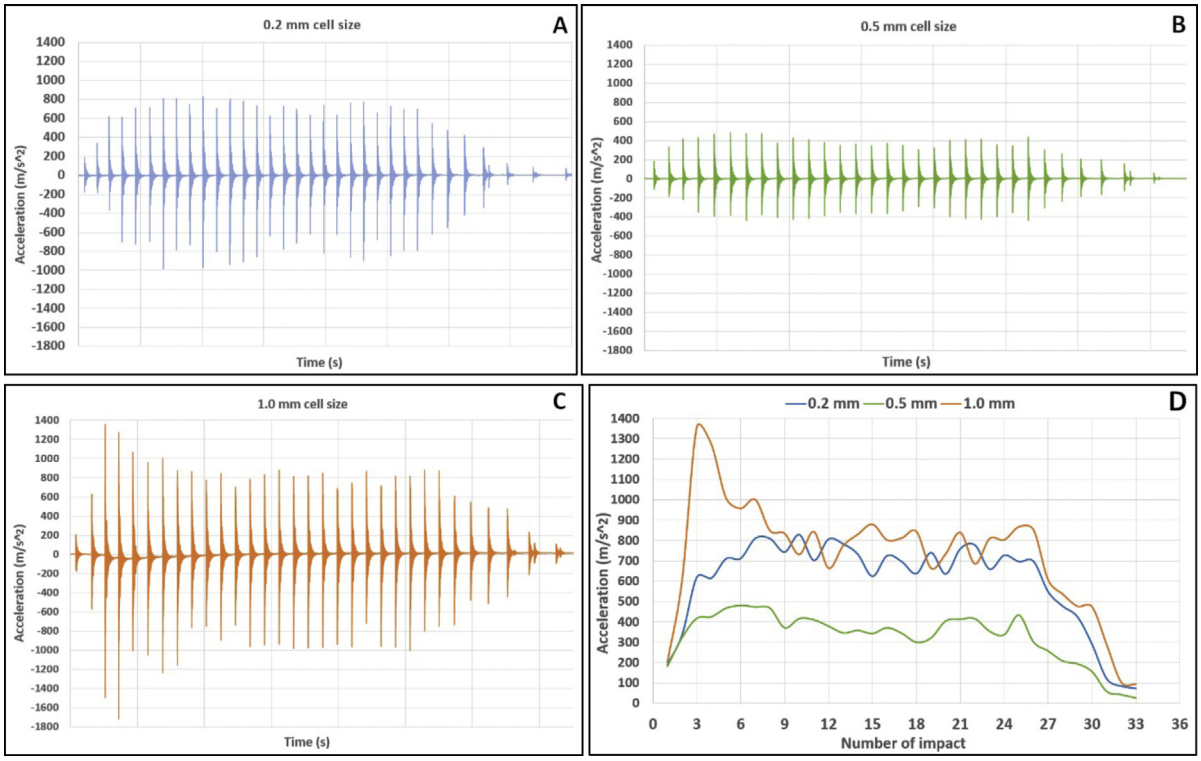

Fig. 8 – Sample acceleration curves for approximately 30 impacts during 1.1 s for composites with strut diameter of: A) 0.2 mm, B) 0.5 mm, and C) 1.0 mm; D) Comparison of positive (during impact) peak values of acceleration.

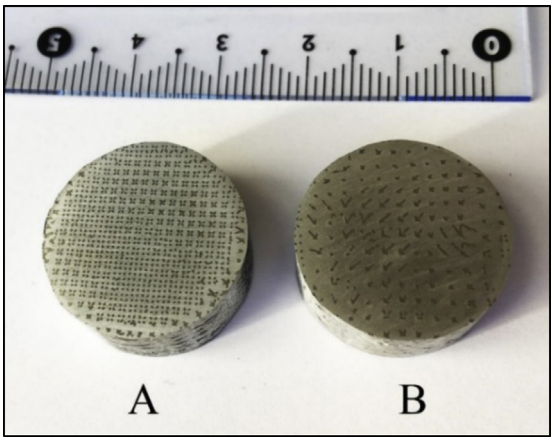

Fig. 9 – Ti6Al4V-AlSi10Mg samples produced by SPS with 45 MPa pressure: A) 1 mm, B) 2 mm cell sizes uniform lattice (both samples have 20 mm diameter and 0.2 mm strut diameter).

3. Results and discussion

Impact wear was tested in a "ball-on-plate" configuration with a modified impact wear device developed in-house [34]. During this test, the sample rigidly fixed to the platform receives repetitive impacts (the impact energy is 5.6 J at a frequency of 27.5 Hz) through a 10 mm diameter zirconia ball (95% ZrO_2 stabilized by 5% Y_2O_3, Tosoh Corporation, Japan). The zirconia ball was used due to its high fracture toughness (in comparison to other commonly used ceramics). The duration of the test was approximately 30 impacts supplied in 1.1 s with an industrial Makita drill. The force pressing the sample against the impacting ball was 98.1 N (10 kg). Vibration (acceleration) monitoring of the platform on which the sample was mounted was measured *in-situ* with a PCH1420 device and an acceleration sensor, PCH-Engineering Denmark. The degree of sample acceleration depends on the loss of energy in the contact zone between the impacting ball and the test sample. The sample that provides a high damping capacity of the impact energy receives the lowest acceleration, while the one that is not able to absorb the energy is accelerated more. The positioning and reciprocation motion of the mechanism is shown in Fig. 5.

ZEISS SteREO discovery V20 motorized Stereo microscope with AxioVision viewer 4.8 software is used to calculate the diameters of regions with multiple impacts (Fig. 6). A similar volume fraction of Ti6Al4V alloy in Ti6Al4V-AlSi10Mg composites is compared to the performance of the composite with smaller cell size and thinner lattice struts (see Fig. 3A) and that of larger cell size and thicker struts mesh (see Fig. 3B). As illustrated in Fig. 6A and 6B, the results on impact (sizes of regions) are quite similar. However, a strut diameter of 1.0 mm gives the best hybrid composite against impact with the smallest size of the region (and also the smallest penetration depth as well) because of the high volume fraction of Ti6Al4V and the thicker struts to absorb the impact energy (Fig. 6C). A structure with uniform distribution and fine mesh lattice can be applied throughout the sample (Fig. 6A), however, for local/overall component reinforcement, structure with thicker struts lattice filled with ductile AlSi10Mg (Fig. 6C) can perform similarly

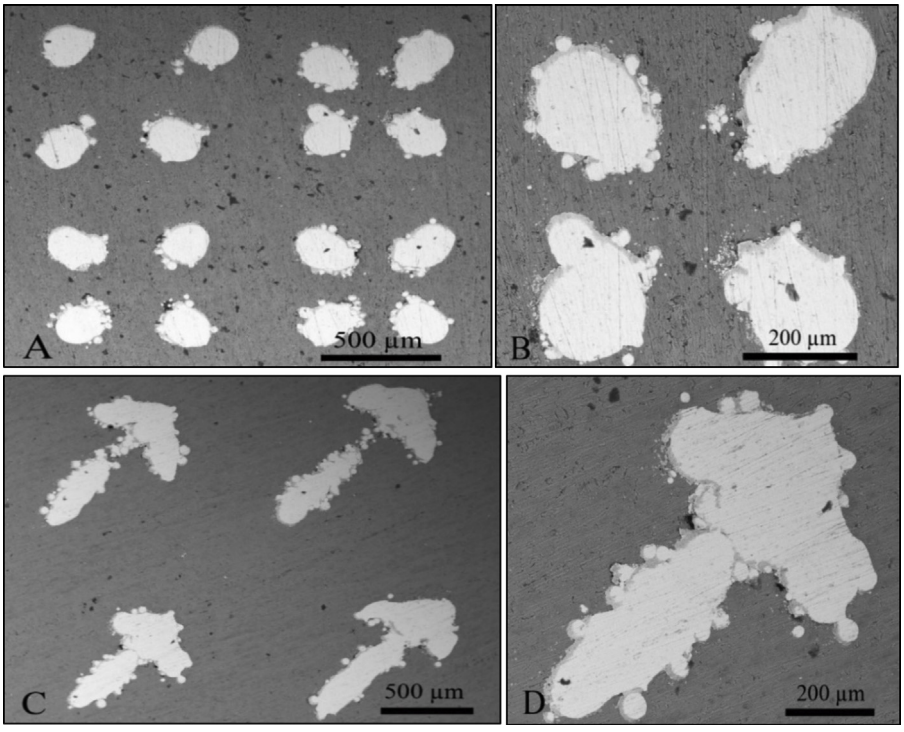

Fig. 10 – SEM micrographs illustrating effect of cell size on deformation of Ti6Al4V-AlSi10Mg samples with equal strut diameter of 0.2 mm sintered under 45 MPa SPS pressure: A and B) 1 mm, C and D) 2 mm with different magnifications. The black pores are graphene sheet pieces survived after course polishing that is used during SPS, inside the graphite mold wall, around and top/bottom sides of sample due to high thermal/electrical conductivity.

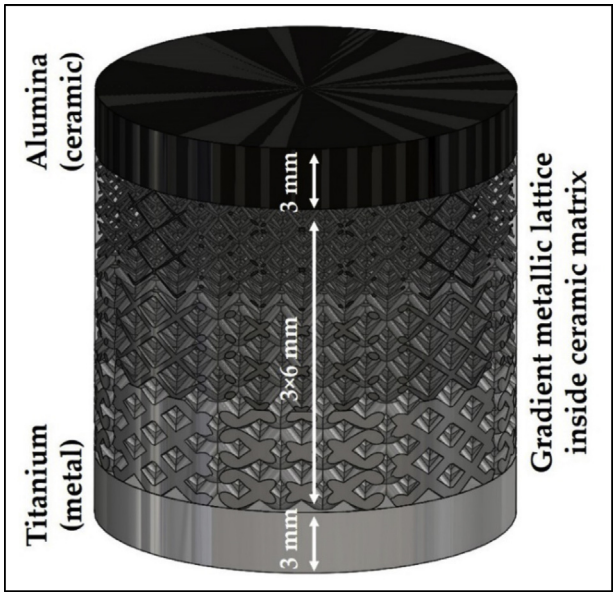

Fig. 11 – An example of possible metal to ceramic gradient material: metal/alloy in bottom (best ductility), metal-ceramic (Al_2O_3 sintered inside Ti6Al4V printed), and pure ceramic in the top (best hardness).

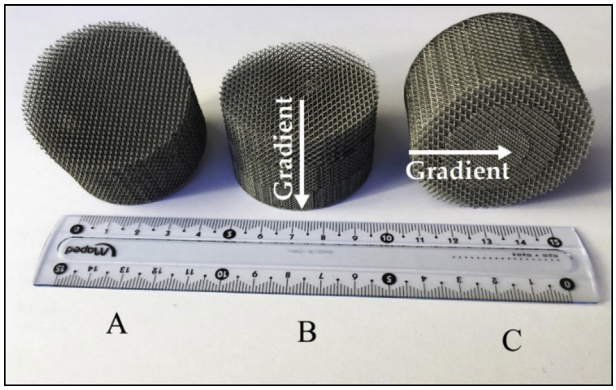

Fig. 12 – Ti6Al4V lattices: A) Uniform 1.5 mm cell size, B) Longitudinal gradient, C) Radial gradient (gradient structures have 1 mm and 45 %, 1.5 mm and 30 % and 2 mm and 15 % cell sizes and volume fraction, respectively; all lattices have 50 mm diameter and 30 mm height). Weight of Ti6Al4V lattices are: A) 20 g, B) 30 g, C) 25 g.

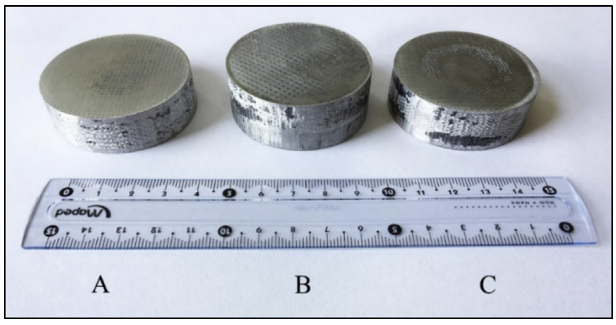

Fig. 13 – Ti6Al4V-AlSi10Mg samples after SPSing: A) Uniform, B) Longitudinal gradient, C) Radial gradient (final height of samples are 14, 18 and 16 mm, respectively). Final weight of samples is around 80 g after polishing, namely A) 20 g + 60 g, B) 30 g + 50 g, C) 25 g + 55 g Ti6Al4V lattice and AlSi10Mg filled powder.

or better than a pure titanium alloy. Note that several studies are focusing on the topology, weight, cell, pore, and strut sizes of lattices, see e.g. [35,36]. The cell sizes $0.75 \times 0.75 \times 0.75\,mm^3$ (Fig. 1A, as a smallest possible cubic dimension for Ti6Al4V powder and SLM50 device) and $2 \times 2 \times 2\,mm^3$ cell (Fig. 1C, as smallest possible cube for 1.0 mm strut) are arbitrary chosen to get "almost identical" proportion of Ti6Al4V metallic lattice (volume fraction around 30–40 %) for samples Figs. 1A and 1B, and "almost two times" for sample Fig. 1C (volume fraction around 70–75 %). The result shows equal deformation for Figs. 6A and 6B, but almost half-deformation for Fig. 6C. An important outcome is independency of formation after impact test from cell size and strut diameter of Ti6Al4V (lattice distribution, relative density) but dependency to the volume fraction of Ti6Al4V in the sample.

Regarding the proximity of the lattice cells to the impact region, the openness of the Ti6Al4V lattice can be accomplished by different rates, see Fig. 7. The cells in Fig. 7C are located near the impact region. The cell size type/architecture has an important role in absorbing the impact energy [37]. The use of Z-BCC (body-centered cubic structure with additional vertical struts in the cell) instead of BCC and redesigned lattice architecture can be investigated in the future to avoid significant deformation of Ti6Al4V cells during impact. Most likely, the ductility of the matrix and the continuation of the lattice have the potential to distribute the impact energy throughout the sample and reduce the stress concentration in the contact region (it can be investigated by the FEA). This explains the impact damping mechanism of the lattice structures. For a future survey on the quality/effectiveness of 3D printed lattices, the strength of the intersection joint of struts can also be investigated.

With this test, we simulate armor piercing and object penetration resistance by approximately 30 sequential impacts applied in a 1.1 s time interval. Figs. 8A-C show acceleration-time curves obtained *in-situ* during the test to evaluate the response of the samples to multiple impacts with a ceramic ball. The lowest acceleration value (highest damping, Fig. 8D) was provided by a composite with 0.5 mm struts, the material with 0.2 mm struts had average performance and the one material with 1.0 mm struts had the highest acceleration (lowest damping) during the first 10 impacts. This is probably because a thicker strut lattice is more rigid and resists against deformation (Ti volume fraction and hardness is greater than Al). This is the perspective of using a gradient structure with uniform and dense mesh in the surface (thinner struts and smaller cell sizes) and a higher volume of Ti6Al4V at the bottom of the structure (thicker struts and larger cell sizes).

To demonstrate the positive effect of low-pressure during SPS, two additional Ti6Al4V-AlSi10Mg samples (with 20 mm diameter and 0.2 mm strut diameter) were produced with

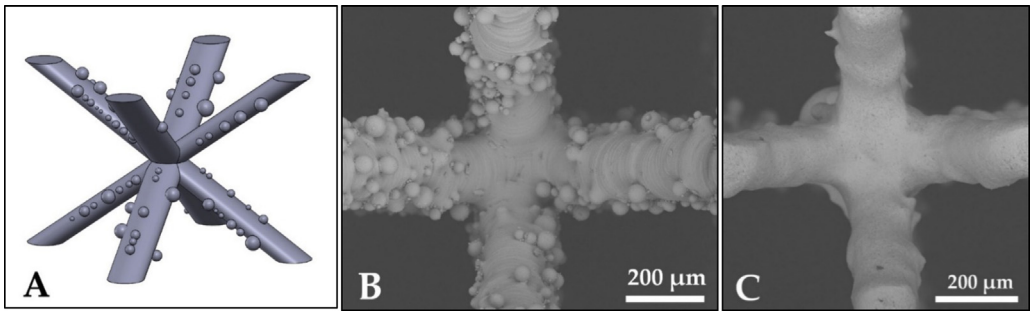

Fig. 14 – A) *SolidWorks* modeled and B) SLM manufactured unit cell size of lattice structure to investigate the effect of unmelted particles in metal-metal or metal-ceramic bonding phase C) Strut cleaning by alumina nanoparticle jet (strut diameters are approximately 0.2 mm).

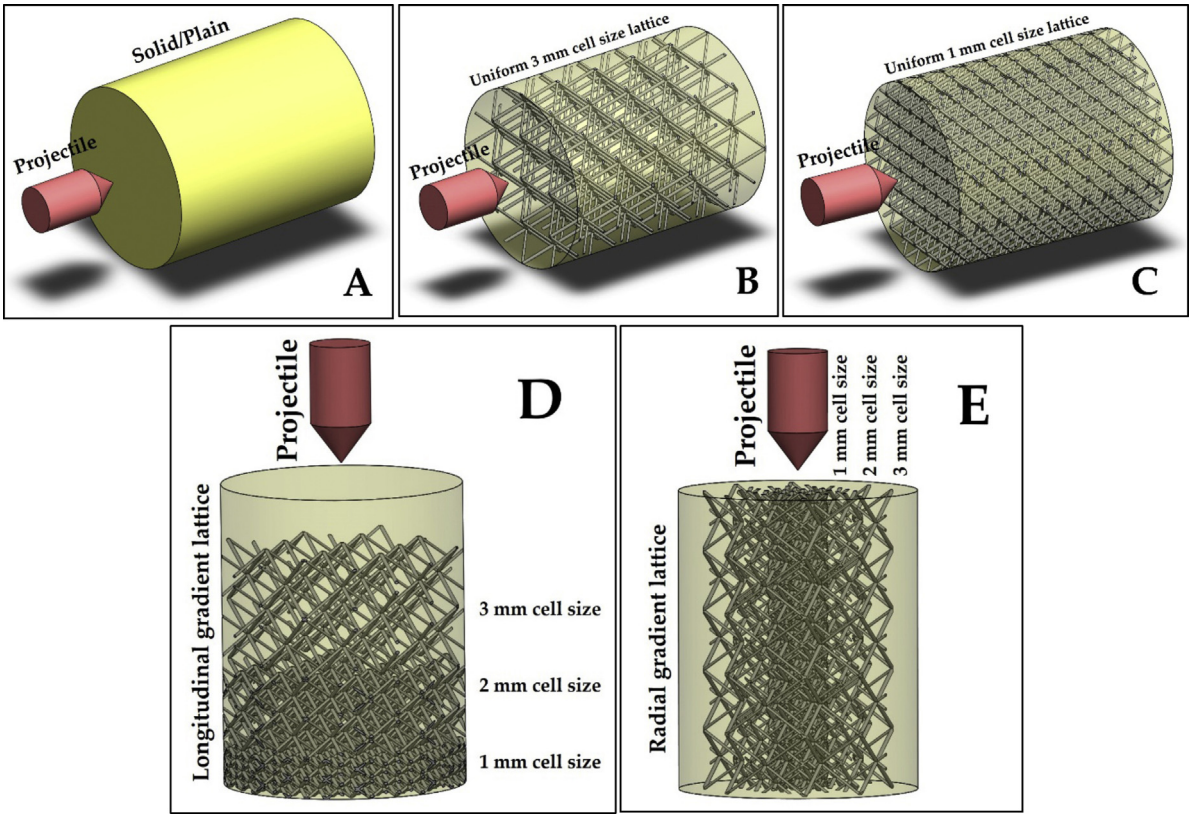

Fig. 15 – Samples designed in *SolidWorks*: A) Solid sample (lattice-free), B) Uniform 3 mm cell size, C) Uniform 1.5 mm cell size, D) Longitudinal gradient, E) Radial gradient lattice structure.

1 mm and 2 mm (previously, the cell size of the tested material with 0.2 mm strut was 0.75 mm) cell sizes, Fig. 9. Compared to samples produced at a lower pressure (15 MPa; Figs. 6,7), samples produced at 45 MPa show higher deformation (Fig. 9 and 10); a higher cell size (2 vs. 1 mm) also leads to increased deformation during the SPS process in terms of bending and buckling of the struts. This means that the failure mechanism should be considered regarding the structure application. Other samples were produced higher pressures and it was concluded that composites with 0.2 mm struts and 1 mm cell size can be successfully sintered without significant deformation at pressure up to 100 MPa.

The titanium alloy is denser and has a higher mechanical strength than AlSi10Mg. In the case of metal-ceramic design, a wide range of 3D printed metal lattices (e.g. 316 L, Ti6Al4V, AlSi10Mg, CuNi2SiCr, CoCr28Mo6, and Inconel718) can be considered as the main impact absorption structure. With regard to the application, the appropriate ceramic (e.g. Al_2O_3, ZrO_2, and TiO_2) can be chosen as the harder matrix. Metallic lattices can be filled gradually by ceramics for AP shield reinforcement (Fig. 11). Gradient cermet structure is the idea of having a pure metal from one side (best ductility), metal-ceramic (e.g. Al_2O_3 sintered inside Ti6Al4V printed) interlayer, and pure ceramic from another side (best hardness).

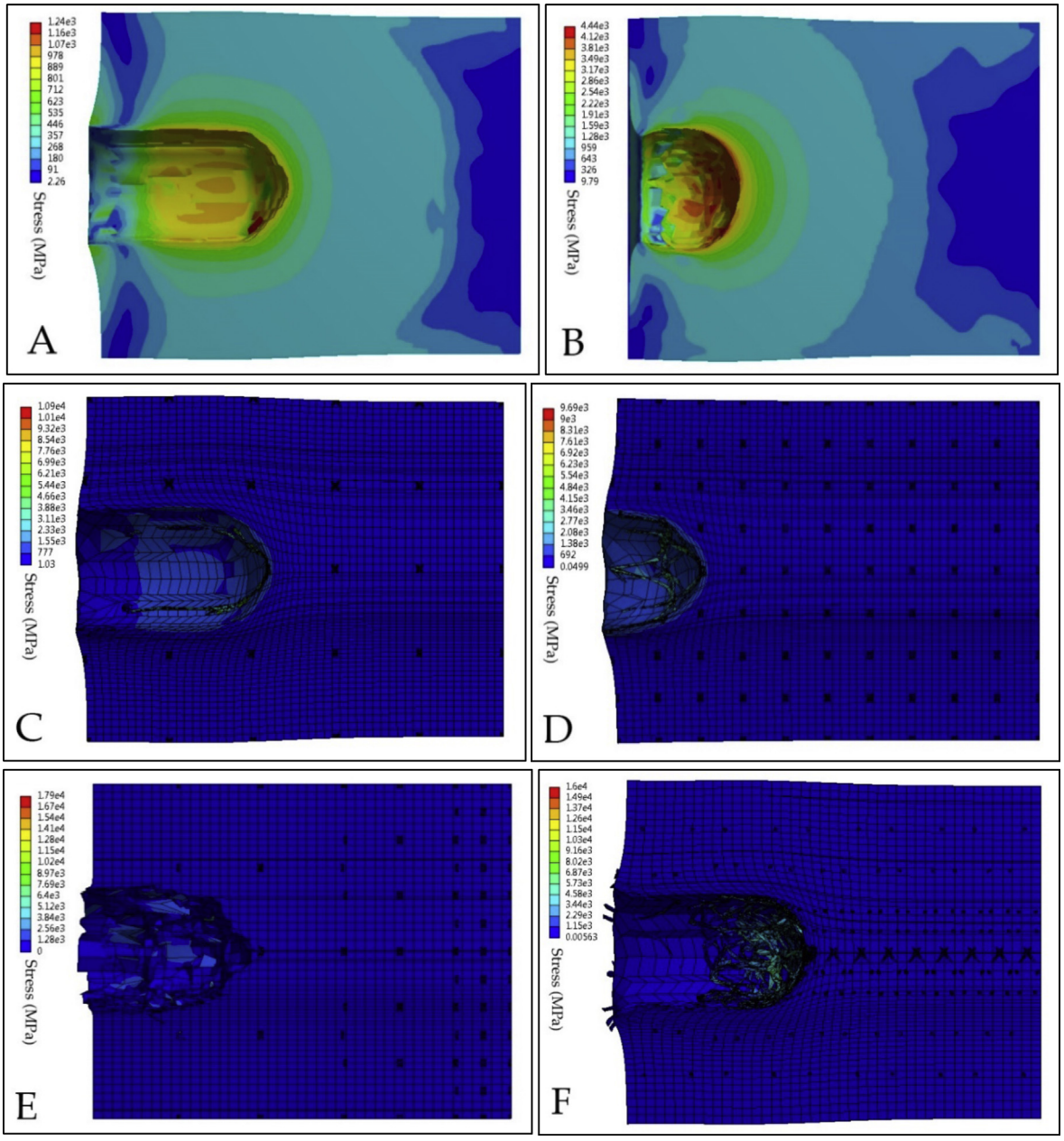

Fig. 16 – Samples subjected to a penetrating object (6.4 g) simulated in *ANSYS* (cross sectional view): A) Solid AlSi10Mg (4.7 g), B) Solid Ti6Al4V (7.8 g), C) Uniform 3 mm cell size Ti6Al4V embedded inside AlSi10Mg (5.7 g), D) Uniform 1.5 mm cell size Ti6Al4V embedded inside AlSi10Mg (7.6 g), E) Longitudinal gradient Ti6Al4V embedded inside AlSi10Mg (4.9 g), F) Radial gradient lattice Ti6Al4V embedded inside AlSi10Mg (4.8 g) structure. Depth of penetration for samples A to F are approximately ≈7.0, 4.5, 6.5, 4.0, 5.5 and 6.0 mm, respectively.

Uniform lattice structure (Fig. 12A), FGL in longitudinal (Fig. 12B), and FGL in radial (Fig. 12C) directions with varied cell sizes (1.0, 1.5, and 2.0 mm) can be considered for directional reinforcement. In order to illustrate the possibility of producing gradient composites, the samples with a 50 mm diameter and 30 mm height were prepared. The final heights (after filling and sintering in SPS) depend on the volume fraction of the lattice, however, the weight of samples is, all the same, about 80 g. Denser mesh/lattice (such as the lowest layer in the longitudinal FGL or the innermost layer in the radial FGL) has a higher resistance and lower shrinkage when subjected to compression/pressure of SPS. Optimized SPS parameters for the Ti6Al4V lattice and AlSi10Mg filled matrix (15 MPa, 500 °C, 5 min) were selected based on experience [28,33]. The samples produced by the SPS process are shown in Fig. 13 (more details are given in figure captions).

SolidWorks modeled lattice (Fig. 14A) adopted from the 3D printed structure (Fig. 14B) can be imported into finite element analysis to investigate the effects of unmelted particles in the metal-metal or the metal-ceramic bonding phase, different cell sizes and strut diameters. Note that the struts can be cleaned/polished with an alumina nanoparticles jet (see

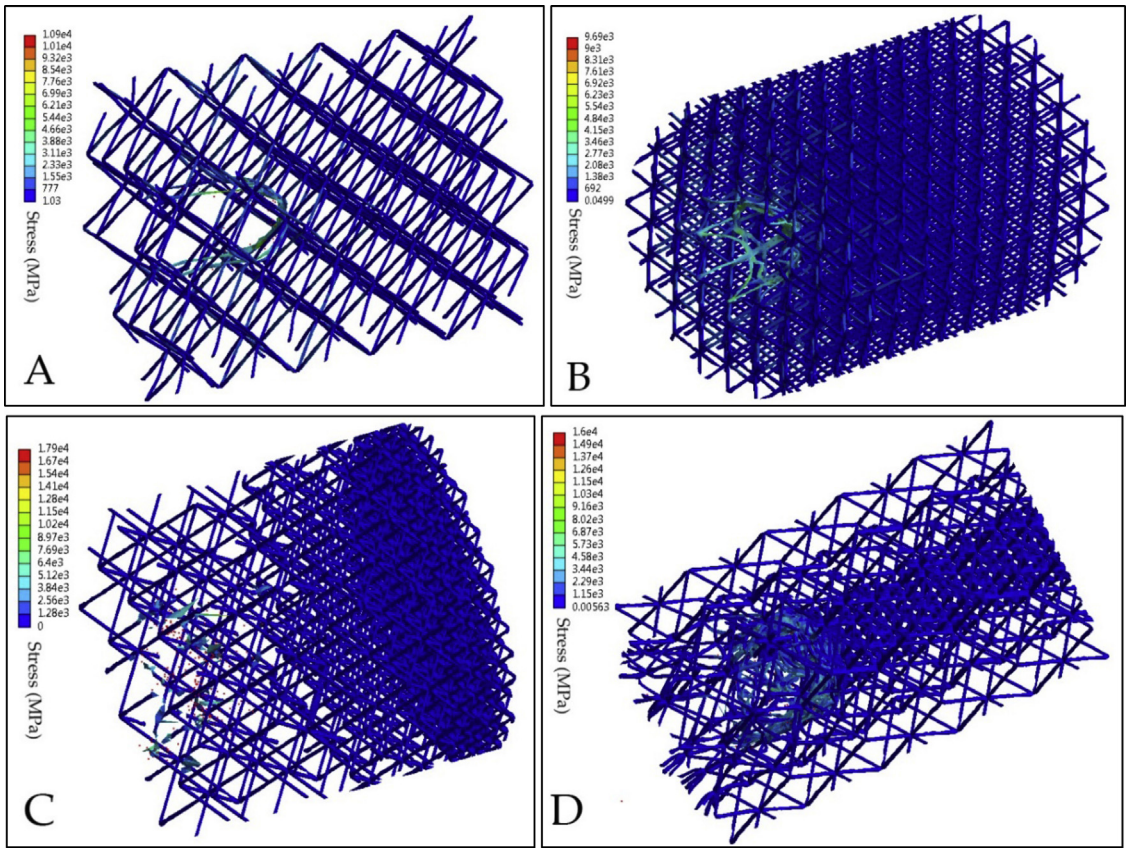

Fig. 17 – Composite samples analyzed by ANSYS. Ti6Al4V lattice structures (without matrix) affected by bullet are presented for: A) Uniform 3 mm cell size, D) Uniform 1.5 mm cell size, E) Longitudinal gradient, F) Radial gradient structure.

Fig. 14C). This is a standard procedure in tissue engineering to prevent unmelted particles. In this case, a combination of gradient porous scaffolds [38], tissue printing [39], impact resistant biomaterials [40] can be the state-of-the-art of in AM science.

4. Simulation study for armor piercing design

FEA is carried out to demonstrate benefits, potential, and ability of the lattice structure subjected to AP for assessment of stress, plastic deformation, and impact absorption properties of Ti-based lattice included matrix than plain Al-based matrix. Five cylindrical samples (Ø12 × 15 mm) are designed, fixed from one side and can deform freely in the axial direction (direction of projectile movement). They are subjected to a penetrating projectile at a speed of 1000 m/s with a height of 6 mm, 3 mm in diameter, and 45° cap angle, schematically shown in Fig. 15. The projectile is modeled as a nonlinear gold alloy with a density of 19.3 g/cm^3 (which is almost the same density of tungsten). A solid sample (no lattice) made from AlSi10Mg or Ti6Al4V (Fig. 15A) is taken as a reference. The second and third samples are modeled as a uniform embedded lattice structure through the whole sample in 3 mm (coarse mesh, Fig. 15B) and 1 mm (dense mesh, Fig. 15C) unit cell size. In all samples, the lattice structures made from Ti6Al4V titanium alloy are filled with the AlSi10Mg matrix. The last two samples are reinforced with a longitudinal (Fig. 15D) and radial (Fig. 15E) FGL structure, which are gradually being designed with 1 mm, 2 mm, and 3 mm unit cell sizes and lattice-free volume at the top or in the periphery of the sample.

For the FEA, a structural explicit dynamic analysis by AUTODYN solver is carried out, the *BEAM188* element type is applied for lattice structure and *SOLID45* for the filled matrix [41,42]. Fig. 16 shows the deformation and Von Mises stress distribution obtained with *ANSYS Workbench v17.2* for six samples: solid AlSi10Mg, solid Ti6Al4V, uniform 3 mm cell size Ti6Al4V embedded inside AlSi10Mg, uniform 1.5 mm cell size Ti6Al4V embedded inside AlSi10Mg, longitudinal gradient Ti6Al4V embedded inside AlSi10Mg and radial gradient lattice Ti6Al4V embedded inside AlSi10Mg. The results show a significant difference between the solid, uniform lattice, and FGL structures, especially in terms of depth of penetration (DOP) and deformation (changing the cylindrical shape of samples). Obviously, the local stress is higher and DOP lower for the Ti6Al4V solid sample (Fig. 16B) than for AlSi10Mg (Fig. 16A). DOP for Al and Ti alloy are 7.0 and 4.5 mm, respectively, and the figures reveal distortion/dislocation of the target at the top of the samples. The coarse distribution of the uniform lattice structure (Fig. 16C) does not show good performance against penetration in comparison with solid AlSi10Mg. However, a finer uniform lattice distribution (Fig. 16D) yields a much better result for stopping the penetrating object and keep the

sample shape undeformed. The maximum stress (usually in the deeper curve area of the bullet-made indent) for samples A to F is 1.24, 4.44, 10.9, 9.69, 17.9, and 16.0 MPa, respectively. Comparing A-B with C–F shows the ability of the lattice structure to concentrate the stress and avoid local stress increment.

In the FGL-included sample (Fig. 16E with 2 mm height for 1 mm cell size, 4 mm height for 2 mm cell size, 6 mm height for 3 mm cell size of the lattice structure and 3 mm lattice-free at the top in uniaxial direction), deformation and stress distribution were higher than for the 1 mm uniform lattice sample (Fig. 16D) but with less distortion in the cylindrical form. This means that the FGL structure absorbs almost all the energy of the impact in the longitudinal direction. Due to the denser agglomeration of Ti6Al4V in the center of the cross-section (3 mm thickness of 1 mm cell size in the innermost radius, 3 mm thickness of 2 mm cell size in the second layer of lattice, 3 mm thickness of 3 mm cell size in the third layer, and 3 mm lattice-free at the outermost radius of the sample in the lateral direction), the response of the radial graded lattice is not good against axial impact (Fig. 16F). It is not cost-effective for local component reinforcement and is not suitable when the displacement of the lattice or the distortion of the outermost layer of the cylinder is to be minimized. Consequently, the finer (with smaller cell size) uniform lattice (Fig. 16D) is best suited to achieve the lowest penetration depth, but the longitudinally graded lattice (Fig. 16E) works best against distortion/deformation. The DOP and weight values for samples 16A to 16 F are approximately (7.0 mm, 4.7 g), (4.5 mm, 7.8 g), (6.5 mm, 5.7 g), (4.0 mm, 7.6 g), (5.5 mm, 4.9 g), and (6.0 mm, 4.8 g), respectively. The lattice structure performance of samples against impact is separately illustrated in Fig. 17.

5. Conclusion

In this paper, a lightweight Ti6Al4V-AlSi10Mg hybrid composite made by a combination of selective laser melting (SLM) and spark plasma sintering (SPS) techniques was studied. 3D printed Ti6Al4V lattice filled with AlSi10Mg and sintered by low-pressure, low-temperature powder metallurgy process. This composite material has been developed to resist impact strikes and armor piercing using a cellular lattice structure (uniform lattice or gradient lattice architecture) using 3D printing technology. In addition, an impact test method has been developed that provides the ability to apply multiple dynamic impacts and *in-situ* measurements of acceleration-time curves (which indicate the damping capability of the composite). The results show the importance of the volume fraction of the Ti6Al4V lattice for the impact resistance. We show that a structure with a smaller cell size and thinner strut diameter has identical performance to a structure with a larger cell size and thicker struts. *SolidWorks* and *ANSYS* software have been combined to model and simulate the penetration depth in lattice-free and lattice-included composites, distortion, deformation, von-Mises stress distribution, and uniform/gradient lattice performance for impact absorption. The finite element results illustrate that a *uniform* lattice structure with a higher volume fraction can more efficiently protect against projectile penetration, while a *gradient* lattice strengthens the material against distortion/deformation to increase damage tolerance.

Conflicts of interest

The authors declare no conflicts of interest.

Acknowledgments

This research was supported by the Estonian Ministry of Education and Research under Projects SS427, PRG643 and M-ERA.NET Duracer ETAG18012, Slovenian Research Agency Program P2-0263.

REFERENCES

[1] Zheng C, Wang F, Cheng X, Fu K, Liu J, Wang Y, et al. Effect of microstructures on ballistic impact property of Ti-6Al-4V targets. Mater Sci Eng A 2014;608:53–62.
[2] Holmen JK, Johnsen J, Jupp S, Hopperstad OS, Børvik T. Effects of heat treatment on the ballistic properties of AA6070 aluminium alloy. Int J Impact Eng 2013;57:119–33.
[3] Alsalla H, Hao L, Smith C. Fracture toughness and tensile strength of 316L stainless steel cellular lattice structures manufactured using the selective laser melting technique. Mater Sci Eng A 2016;669:1–6.
[4] Lewandowski JJ, Seifi M. Metal additive manufacturing: a review of mechanical properties. Annu Rev Mater Res 2016;46:151–86.
[5] Liu J, Gaynor AT, Chen S, Kang Z, Suresh K, Takezawa A, et al. Current and future trends in topology optimization for additive manufacturing. Struct Multidiscip Optim 2018;57:2457–83.
[6] Zhang S, Lane B, Whiting J, Chou K. On thermal properties of metallic powder in laser powder bed fusion additive manufacturing. J Manuf Process 2019;47:382–92.
[7] Ngo TD, Kashani A, Imbalzano G, Nguyen KTQ, Hui D. Additive manufacturing (3D printing): a review of materials, methods, applications and challenges. Compos Part B Eng 2018;143:172–96.
[8] Liu S, Shin YC. Additive manufacturing of Ti6Al4V alloy: a review. Mater Des 2019;164:107552.
[9] Girelli L, Giovagnoli M, Tocci M, Pola A, Fortini A, Merlin M, et al. Evaluation of the impact behaviour of AlSi10Mg alloy produced using laser additive manufacturing. Mater Sci Eng A 2019;748:38–51.
[10] Fiegl T, Franke M, Körner C. Impact of build envelope on the properties of additive manufactured parts from AlSi10Mg. Opt Laser Technol 2019;111:51–7.
[11] Vasylyev MA, Chenakin SP, Yatsenko LF. Ultrasonic impact treatment induced oxidation of Ti6Al4V alloy. Acta Mater 2016;103:761–74.
[12] Dekhtyar AI, Mordyuk BN, Savvakin DG, Bondarchuk VI, Moiseeva IV, Khripta NI. Enhanced fatigue behavior of powder metallurgy Ti-6Al-4V alloy by applying ultrasonic impact treatment. Mater Sci Eng A 2015;641:348–59.
[13] Holovenko Y, Kollo L, Saarna M, Rahmani R, Soloviova T, Antonov M, et al. Effect of lattice surface treatment on performance of hardmetal-titanium interpenetrating phase composites. Int J Refract Metals Hard Mater 2020;86:105087.
[14] Kamboj N, Kazantseva J, Rahmani R, Rodríguez MA, Hussainova I. Selective laser sintered bio-inspired silicon-wollastonite scaffolds for bone tissue engineering. Mater Sci Eng C 2020;116:111223.
[15] Rahmani R, Rosenberg M, Ivask A, Kollo L. Comparison of mechanical and antibacterial properties of TiO_2/Ag ceramics

and Ti6Al4V-TiO_2/Ag composite materials using combining SLM-SPS techniques. Metals 2019;9:874.
[16] Kamboj N, Rodríguez MA, Rahmani R, Prashanth KG, Hussainova I. Bioceramic scaffolds by additive manufacturing for controlled delivery of the antibiotic vancomycin. Proc Estonian Acad Sci Biol Ecol 2019;68:185–90.
[17] Rahmani R, Antonov M, Kollo L, Holovenko Y, Prashanth KG. Mechanical behavior of Ti6Al4V scaffolds filled with $CaSiO_3$ for implant applications. Appl Sci (Basel) 2019;9:3844.
[18] Calignano F. Design optimization of supports for overhanging structures in aluminum and titanium alloys by selective laser melting. Mater Des 2014;64:203–13.
[19] Brandl E, Heckenberger U, Holzinger V, Buchbinder D. Additive manufactured AlSi10Mg samples using Selective Laser Melting (SLM): Microstructure, high cycle fatigue, and fracture behavior. Mater Des 2012;34:159–69.
[20] Zhang ZH, Liu ZF, Lu JF, Shen XB, Wang FC, Wang YD. The sintering mechanism in spark plasma sintering; Proof of the occurrence of spark discharge. Scr Mater 2014;81:56–9.
[21] Diouf S, Molinari A. Densification mechanisms in spark plasma sintering: effect of particle size and pressure. Powder Technol 2012;221:220–7.
[22] Bürger D, de Faria AR, de Almeida SFM, de Melo FCL. Ballistic impact simulation of an armor-piercing projectile on hybrid ceramic/fiber reinforced composite armors. Int J Impact Eng 2012;43:63–77.
[23] Krishnan K, Sockalingam S, Bansal S, Rajan SD. Numerical simulation of ceramic composite armor subjected to ballistic impact. Compos Part B Eng 2010;41:583–93.
[24] Senthil K, Iqbal MA. Effect of projectile diameter on ballistic resistance and failure mechanism of single and layered aluminum plates. Theor Appl Fract Mech 2013;67-68:53–64.
[25] Feli S, Asgari MR. Finite element simulation of ceramic/composite armor under ballistic impact. Compos Part B Eng 2011;42:771–80.
[26] Hubert W, Meyer Jr, Kleponis DS. Modeling the high strain rate behavior of titanium undergoing ballistic impact and penetration. Int J Impact Eng 2001;26:509–21, https://www.slm-solutions.com/en/.
[27] Rahmani R, Antonov M, Kollo L. Wear resistance of (Diamond-Ni)-Ti6Al4V gradient materials prepared by combined selective laser melting and spark plasma sintering techniques. Adv. Tribol 2019:5415897.
[28] Rahmani R, Brojan M, Antonov M, Prashanth KG. Perspectives of metal-diamond composites additive manufacturing using SLM-SPS and other techniques for increased wear-impact resistance. Int J Refract Metals Hard Mater 2020;88:105192.
[29] Li C, Lei H, Zhang Z, Zhangc Xiaoyu, Zhou H, Wang P, et al. Architecture design of periodic truss-lattice cells for additive manufacturing. Addit Manuf 2020;34:101172.
[30] Al-Ketan O, Rowshan R, Al-Ruba RKA. The effect of architecture on the mechanical properties of cellular structures based on the IWP minimal surface. Materials Research Society 2018;33, http://www.fct-systeme.de/en/.
[31] Rahmani R, Antonov M, Kollo L. Selective Laser Melting of Diamond-Containing or Postnitrided Materials Intended for Impact-Abrasive Conditions: Experimental and Analytical Study. Adv Mater Sci Eng Int J 2019:4210762.
[32] Antonov M, Veinthal R, Yung DL, Katusin D, Hussainova I. Mapping of impact abrasive wear performance of WC-Co cemented carbides. Wear 2015;332-333:971–8.
[33] Al-Ketana O, Rowshan R, Al-Ruba RKA. Topology-mechanical property relationship of 3D printed strut, skeletal, and sheet based periodic metallic cellular materials. Addit Manuf 2018;19:167–83.
[34] Yan C, Hao L, Husseina A, Bubb SL, Young P, Raymont D. Evaluation of light-weight AlSi10Mg periodic cellular lattice structures fabricated via direct metal laser sintering. J Mater Process Technol 2014;214:856–64.
[35] Rahmani R, Antonov M, Kamboj N. Modelling of impact-abrasive wear of ceramic, metallic, and composite materials. Proc Estonian Acad Sci Biol Ecol 2019;68:191–7.
[36] Baruia S, Chatterjee S, Mandal S, Kumar A, Basu B. Microstructure and compression properties of 3D powder printed Ti-6Al-4V scaffolds with designed porosity: experimental and computational analysis. Mater Sci Eng C 2017;70:812–23.
[37] Kamboj N, Aghayan M, Rodrigo-Vazquezc CS, Rodríguez MA, Hussainova I. Novel silicon-wollastonite based scaffolds for bone tissue engineering produced by selective laser melting. Ceram Int 2019;45:24691–701.
[38] Grunenfelder LK, Suksangpanya N, Salinas C, Milliron G, Yaraghi N, Herrera S, et al. Bio-inspired impact-resistant composites. Acta Biomater 2014;10:3997–4008.
[39] Cerardi A, Caneri M, Meneghello R, Concheri G, Ricotta M. Mechanical characterization of polyamide cellular structures fabricated using selective laser sintering technologies. Mater Des 2013;46:910–5.
[40] Terriault P, Brailovski V. Modeling and simulation of large, conformal, porosity-graded and lightweight lattice structures made by additive manufacturing. Finite Elem Anal Des 2018;138:1–11.